Materials and Structures, 1994, **27**, 99–105

A general bilinear fit for the softening curve of concrete

G. V. GUINEA, J. PLANAS, M. ELICES

Departamento de Ciencia de Materiales, Escuela de Ingenieros de Caminos, Universidad Politécnica, Ciudad Universitaria, 28040 Madrid, Spain

The softening function is the main input needed to model the fracture of concrete when using a cohesive crack approach. The simplest softening function that describes concrete behaviour reasonably well is a bilinear one. It is defined by four parameters: the tensile strength f_t, the specific fracture energy G_F, and two parameters characterizing the shape of this function. Here it is shown how these parameters can be derived from experimental measurements on notched beam tests. In particular, the parameters characterizing the shape of the function come from knowledge of the tail of the load–displacement curve and from the recorded maximum loads when similar beams of different sizes are tested.

1. INTRODUCTION

Modelling concrete fracture by using cohesive cracks has been a successful procedure since its proposal by Hillerborg *et al.* [1]. This success is partly due to its physical meaning and to its simplicity. A basic ingredient of the model is the *softening* curve, a material property. This function relates the stresses acting across the crack faces – the cohesive stresses – to the corresponding crack openings.

The area under the softening function is known as the *specific fracture energy*, G_F, and it is also a material property. G_F measures the energy needed to completely break a unit area, and RILEM Committee TC-50 has published a proposal, based on three-point bend tests in notched beams, to measure this property [2].

Available measurements of the specific fracture energy G_F obtained with the RILEM procedure provide values that appear to increase with increasing sample size [3], calling into question the consideration of G_F as a material parameter, and the softening function as well. This size effect on G_F was analysed by the authors [4–6], and it was concluded that if all the sources of spurious energy dissipation were taken into account, and when the energy at the very end of the test was not neglected, the corrected values of G_F are nearly independent of size. These findings provide additional support for G_F and for the softening function as material properties and, as a consequence, for the use of cohesive cracks to model cracking.

The input required for cohesive crack computations is the softening function. Ideally, the simplest method of obtaining this curve should be to perform direct tensile tests but unfortunately this procedure has many drawbacks [7, 8] because it is very difficult to propagate cracks in a stable and symmetric way. This is why most of the procedures to infer the softening function rely on indirect methods based on a parametric fit of the experimental results from bending beams or compact specimens [9, 10].

This paper presents a novel procedure for inferring the essential properties of the softening function from tests performed on notched beams. Any softening function depending on up to four parameters may be envisaged, but this paper focuses on a bilinear relationship, with four degrees of freedom. Four essential geometrical parameters are shown to be easily estimated from classical tests (ASTM tests for elastic modulus and splitting tensile strength, and the RILEM work-of-fracture recommendation for fracture energy).

The procedure for finding those parameters is applied to experimental results previously obtained by the authors, and the resulting softening curve, which happens to present a long tail, is compared with other bilinear approximations found in the literature. The essential result is that any of these approximations gives a good prediction of stable tests on notched beams in the pre-peak and near post-peak region, but that only the long-tailed bilinear softening fits also the post- and far post-peak region.

2. EXPERIMENTAL RESULTS FOR CONCRETE

For clarity, the softening function for a particular concrete will be derived from experimental measurements already performed by the authors, but the procedure is general. Apart from measurements of the tensile strength and the specific fracture energy, one needs a recording of the tail of the load–displacement curve in a notched beam test and a knowledge of the maximum load size effect for a range of usual sizes.

Tests were performed on concrete notched beams, following essentially the RILEM recommendations for the measurement of G_F [2]. Details of materials and experimental procedures have already been published [11] and therefore only the relevant aspects are summarized here.

The concrete was a standard RILEM concrete as described by Dutron [12]. The cement was of ASTM type III, and the aggregates were classified as siliceous and natural rounded, of maximum size 10 mm. Table 1

0025-5432/94

Table 1 Concrete properties

Proportional mixing, by weight[a]				Concrete strength (MPa)[b]		
Cement	Coarse	Fine	Water	Compressive	Tensile	Modulus
1.00	1.35	3.02	0.55	33.1	2.8	26 600

[a] Cement content 400 kg m^{-3}.
[b] Strength results at 28 days.

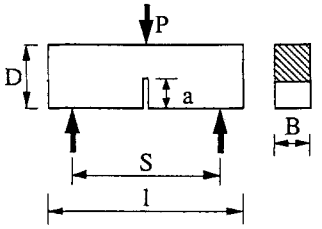

Size	l	S	D	a	B
IV	800	750	300	100	100
III	550	500	200	67	100
II	550	250	100	33	100
I	300	125	50	17	100

in mm

Fig. 1 Specimen geometry.

summarizes the characteristics of the concrete mix and some concrete properties according to ASTM standards.

The test specimens were notched beams, as sketched in Fig. 1. All specimens were cast in steel moulds and compacted with a vibrating table. After demoulding, the samples were stored under lime-saturated water until testing time.

Testing was performed in a 1 MN servohydraulic testing machine (Instron 1275) run in CMOD control mode. Loads were measured with a 25 kN load cell with a resolution of 1.25 N and 0.5% accuracy. CMOD was measured by a clip-on gauge (MTS 632.03C-51) with ± 2 μm accuracy.

Deflection was measured as the relative displacement of the central loading head and the line defined by the points of the upper surface of the specimen located on the verticals of the lower supports. The displacement was measured by an extensometer located in a transverse hole in the loading head. The accuracy of the extensometer was better than 5 μm.

In all tests, weight compensation was used. This was automatically accomplished by using specimens twice as long as the loading span for the two smallest sizes. Prestressed springs on both sides of the notch provided the load compensation for the larger specimens.

For every test, load, displacement and CMOD were recorded. Tests were run on CMOD control. The average values of maximum loads for every size are shown in Table 2.

Table 2 Maximum load values

Size	Beam depth (mm)	P_{max} (kN)
I	50	2.89 ± 0.05
II	100	5.21 ± 0.06
III	200	9.37 ± 0.06
IV	300	11.25 ± 3.08

3. INFERENCE OF THE SOFTENING FUNCTION

The softening function will be approximated by a bilinear function. This simple diagram captures the essential facts: large-scale debonding, or fracture, of aggregates in the steepest part, and frictional pull-out of aggregates in the shallow tail of the diagram. This function is completely characterized when the following four parameters are known, as shown in Fig. 2: the tensile strength f_t, the

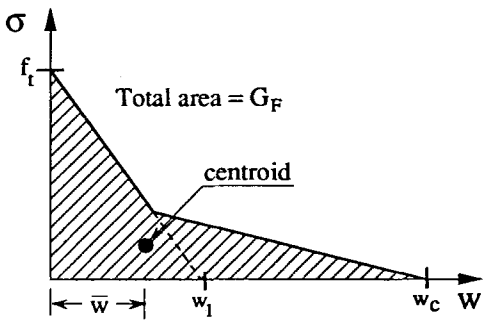

Fig. 2 Bilinear softening function.

specific fracture energy G_F, the abscissa of the centroid of the softening area $\bar{w}$, and the initial slope, measured as the horizontal intercept w_1 of the steeper segment. Nevertheless, the proposed method of inferring the softening function can also be used for functions other than bilinear ones, provided they are characterized by four independent parameters.

3.1 Tensile strength f_t

As already mentioned, direct tensile tests are difficult to perform, and their results are not always free of spurious influences. When no reliable direct tension tests were available, the authors used the result of a Brazilian splitting test (ASTM C-495) as an estimate of the tensile strength (assumed a material property if one accepts the cohesive crack model). One must be aware that this is a simplification of the experimental procedure, and that the error in the estimation depends on the size of the cylindrical specimens used and, most importantly, on the brittleness of the concrete. This subject will be further addressed in the discussion of the fitting method, in section 4. For the concrete of our example the cylinder

Table 3 Specific fracture energy determination

Source	Size I	Size II	Size III	Size IV
G_{FMeas}	57 ± 2	75 ± 13	82 ± 2	94 ± 5
$-\Delta G_{Fhyst.}$	0	−0.2	−0.2	−0.5
$-\Delta G_{Fbulk}$	−0.5 (0.2)[a]	−1.0 (0.3)	−1.5 (0.4)	−1.7 (0.5)
$-\Delta G_{Fsupports}$	−7.3 (2.5)	−6.6 (2.0)	−8.6 (2.3)	−9.2 (1.6)
$+\Delta G_{Ftail}$	22.0 (8.0)	18.0 (8.0)	7.0 (2.0)	6.0 (4.0)
G_F	71 [13][b]	85 [23]	79 [7]	89 [11]

[a] Standard deviation.
[b] Estimated variation interval.

splitting tests delivered $f_t \simeq f_s = 2.8$ MPa, where f_s stands for the (cylinder) splitting strength.

3.2 Specific fracture energy G_F

The area enclosed under the softening function is the specific fracture energy G_F. This parameter was measured according to the RILEM procedure [2] with some improvements [4–6]. Basically, G_F was obtained by dividing the measured work of fracture W by the ligament area:

$$G_{FMeas} = \frac{W}{Bb} \tag{1}$$

where b is the initial ligament length; $b = D - a$ according to Fig. 1.

These G_{FMeas} results show a clear size effect, increasing with specimen size. When sources of spurious energy dissipation – hysteresis of the testing equipment, volume dissipation and energy dissipation at the supports – and the effect of interrupting the test at some fixed rotation angle are taken into account, an almost size-independent G_F emerges. This corrected value, for our concrete, was $G_F = 81$ N m^{-1}. Table 3 summarizes the experimental results and the corrections that take into account the above-mentioned sources of energy.

3.3 Abscissa of the centroid of the softening curve, $\bar{w}$

In a previous paper [6] it was shown that the abscissa $\bar{w}$ of the centroid of the area under the softening curve can be evaluated from a knowledge of the load–displacement (P–δ) tail recorded during experimentation. Very briefly, the reasoning is as follows: for cohesive materials and beams where *the self-weight is compensated*, the last phase of a stable three-point bend test can be modelled by rigid-body kinematics. If $\sigma(w)$ is the softening function, the bending moment per unit thickness at the central section, M, may be approximated by

$$M = \int_0^{z_c} \sigma[w(z)]z \, dz \simeq \frac{1}{\theta^2} \int_0^{w_c} \sigma(w)w \, dw = \frac{1}{\theta^2} \bar{w} G_F \tag{2}$$

where z and θ are shown in Fig. 3 and z_c is the point where the softening is complete, i.e. $w(z_c) = w_c$; the second integral follows by setting $\theta z \simeq w$, the rigid-body

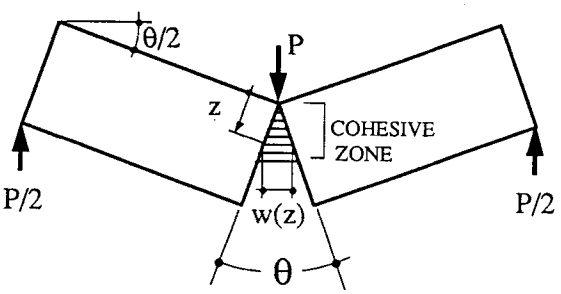

Fig. 3 Rigid-body kinematics at the end of the test.

kinematics approximation; the last expression just states that the second integral in Equation 2 is the first-order moment of $\sigma(w)$ and can be expressed as the area enclosed between the positive axes and the softening curve, G_F, times the abscissa, $\bar{w}$, of the centroid of that area.

The centroid of the area may be always written in the form

$$\bar{w} = \frac{\alpha G_F}{f_t} \tag{3}$$

α is a dimensionless parameter depending on the shape of the softening function. For rectangular softening $\alpha = 1/2$, for linear softening $\alpha = 2/3$, for exponential softening $\alpha = 1$, also $\alpha = 0.987$ for the bilinear softening proposed by Petersson [13] and between 1 and 1.3 for the functions proposed by Reinhardt *et al.* [7]. As a general trend, α values increase with the importance of the P–δ tail.

From the recorded tails of the P–δ curves, the M–θ curves were evaluated and an α value of 2.1 was obtained as detailed elsewhere [6]. The abscissa $\bar{w}$, for our concrete, was $\bar{w} \simeq 61$ μm.

3.4 Initial tangent intercept w_1

In a previous paper [14] the authors compared the maximum load predictions in notched-beam tests for different softening functions, considering particularly the linear softening and quasi-exponential softening. It was found that both models could be led to give essentially the same values of the maximum load for sizes in the practical experimental range (beam depths between 0.1 and 0.4 m). Differences were below ±3%, a value well

inside the experimental scatter band for maximum load determination in concrete testing.

This result is so because, as already shown by Petersson [13], except for very large specimen sizes the peak load is reached well before any point in the cohesive zone undergoes complete softening, which means that as far as the peak load is concerned and as long as not too large a specimen is used, only the initial portion of the softening curve is important. In particular, for bilinear softening and a small enough specimen, the peak load must exactly coincide with that for linear softening with the same horizontal intercept w_1, represented by the dashed line in Fig. 2. This fact may be exploited to devise a simple procedure to find w_1 from the experimentally measured peak loads, as shown below.

Consider the variation with size of the maximum load of a family of geometrically similar specimens, i.e. the size effect. As shown by the authors [14], given the geometry and a softening function depending on two parameters, such as the linear or the Petersson softening functions, the size-effect curve is unique if represented in non-dimensional form. In the case of linear softening, this curve may be written as

$$\frac{\sigma_{\mathrm{Nmax}}}{f_t} = \psi\left(\frac{2Df_t}{Ew_1}\right) \tag{4}$$

where E is the elastic modulus, D the beam depth, w_1 the critical opening, and σ_{Nmax} the peak nominal stress defined, for three-point bending, as

$$\sigma_{\mathrm{N}} = \frac{3}{2}\left(\frac{PS}{BD^2}\right) \qquad \sigma_{\mathrm{Nmax}} = \frac{3}{2}\left(\frac{P_{\max}S}{BD^2}\right) \tag{5}$$

where $P_{\max}$ is the maximum load and the dimensions S, B and D are as shown in Fig. 1.

The essential point is that the function ψ in Equation 4 is unique and may be found once and for all by using a suitable computational method using arbitrary values of f_t, E and w_1. We have computed this curve for the geometry in Fig. 1 using the influence method, which is described in detail elsewhere [15]. The resulting curve, called the 'master curve', has been plotted in a semilog–log plot in which the abscissa x_{M} (M stands for master) and ordinate y are given by

$$x_{\mathrm{M}} = \log\left(\frac{2Df_t}{Ew_1}\right) \qquad y = \frac{\sigma_{\mathrm{Nmax}}}{f_t} \tag{6}$$

The resulting master curve is plotted in Fig. 4 as a full line.

The problem now is to find a particular value of w_1 such that the experimental values of the peak load, for the given experimental sizes, fit the theoretical prediction just presented. This is easily accomplished if one represents the experimental points in the same plot as the master curve, using the same ordinate, but an abscissa x given by

$$x = \log\left(\frac{Df_t^2}{EG_{\mathrm{F}}}\right) \tag{7}$$

where all the parameters appearing in the expression have been measured.

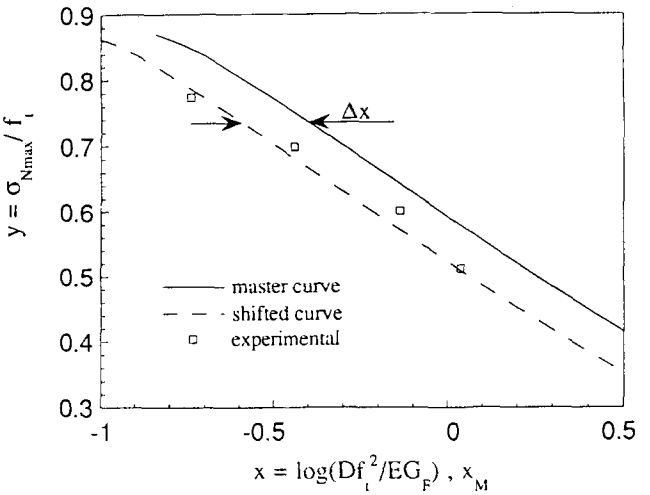

Fig. 4 Peak-load size effect for linear softening.

Comparing Equations 6 and 7 it turns out that the abscissae of the experimental points are related to the abscissae of the master curve (for identical ordinates) by

$$x = x_{\mathrm{M}} - \Delta x \qquad \Delta x = \log\left(\frac{2G_{\mathrm{F}}}{w_1 f_t}\right) \tag{8}$$

which means that the experimental results should lie on a curve which is obtained by shifting the master curve by a magnitude Δx towards the left as shown in Fig. 4 by the dashed line. As derived from this figure, the greater Δx the more appropriate is the use of bilinear softening instead of linear to model the material.

Graphical evaluation of Δx leads to the immediate determination of w_1, since from Equation 8 we have

$$w_1 = \frac{2G_{\mathrm{F}}}{f_t}\,10^{-\Delta x} \tag{9}$$

which for the particular case of our tests delivers a value $w_1 = 1.28\ G_{\mathrm{F}}/f_t = 37\ \mu\mathrm{m}$.

3.5 General bilinear fit (GBF) for the softening function

The bilinear softening function for the concrete utilized in our tests can be derived from the four parameters obtained in the preceding paragraph. These results are:

$f_t = 2.8$ MPa from Brazilian tests (ASTM C-495)
$G_{\mathrm{F}} = 81\ \mathrm{N\,m^{-1}}$ from the load–displacement curve (RILEM procedure plus corrections)
$\bar{w} = 61\ \mu\mathrm{m}$ from the tail of load–displacement curves
$w_1 = 37\ \mu\mathrm{m}$ from the maximum load size effect

From these results and some simple geometrical relationships shown in the Appendix the characteristic points of the bilinear curve can be easily obtained. The critical crack opening turns out to be $w_{\mathrm{c}} = 12.7\ G_{\mathrm{F}}/f_t = 367\ \mu\mathrm{m}$, and the coordinates of the kink point $w_{\mathrm{k}} = 34.7\ \mu\mathrm{m}$ and $\sigma_{\mathrm{k}} = 0.176$ MPa.

4. DISCUSSION AND CONCLUSIONS

4.1 Results of the fit

Fig. 5 compares the general bilinear fit for the softening curve (GBF) with those of Petersson [13] and Rokugo *et al.* [16] which depend only on two parameters (f_t and G_F). It is obvious that our fit displays a much longer tail than the other two. Notice, however, that the initial segments of the softening curves are very close to each other. This is why, as explained before, the three softenings fit the experimental results very well as far as the peak load is concerned and as long as the specimens are not too large.

This is clearly shown in Fig. 6 where the peak loads for different specimen sizes are plotted (in a convenient dimensionless plot) as given by the experiments and as predicted by the three bilinear softenings shown in Fig. 5. The characteristic length l_{ch}, used to make the size non-dimensional, is a material property and was defined by Hillerborg [3] as

$$l_{ch} = \frac{EG_F}{f_t^2} \tag{10}$$

For the concrete used (E = 26.6 GPa, f_t = 2.8 MPa and G_F = 81 N m^{-1}), the characteristic length is 0.275 m. As expected, the agreement between experimental results and all the numerical predictions is excellent. The model of Rokugo *et al.* predicts a somewhat lower strength (by about 5%) because the slope of the initial softening segment is larger (about 37% larger than for GBF).

Pushing the comparison a little further, Fig. 7 shows the dimensionless load–CMOD curves for beams of 100 mm depth. The experimental curve is the average of two tests. Up to the maximum load, the Petersson model and ours (GBF) give the same values and agree quite well with the experimental result. As seen in the figure, the model of Rokugo *et al.* predicts lower loads than the other two bilinear functions, as expected according to previous comments. It is in the post-peak region that the predictions of the models differ. Our predictions still fit the experimental results. The Petersson model predicts higher loads, mainly because it was not derived for the purpose of fitting the far end of the test. The softening function of Rokugo *et al.*, having an intermediate critical crack opening, leads to results between Petersson's and ours.

The large value of the critical crack opening w_c = 12.7 G_F/f_t = 367 μm obtained in our experiments deserves some additional comments. This value is larger than those currently appearing in models quoted in the literature. However, recent experimental results tend to support values of w_c in accordance with our findings; see for example van Mier [17] in direct tensile tests with concrete using aggregates of 16 mm, or the Rokugo *et al.* results [16] using the tube tension test which yielded values of w_c around 10.8 G_F/f_t = 460 μm for concrete with aggregates of 15 mm maximum size. In a recent paper, Liaw *et al.* [18] proposed a bilinear diagram with w_c between 3.6 and 4.6 G_F/f_t, claiming that numerical

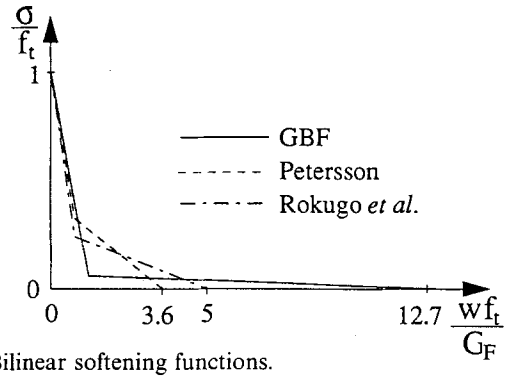

Fig. 5 Bilinear softening functions.

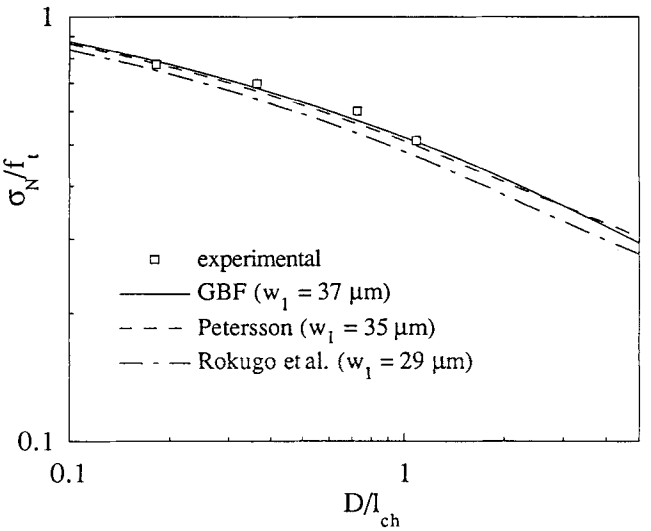

Fig. 6 Peak-load size effect; experimental data and model predictions.

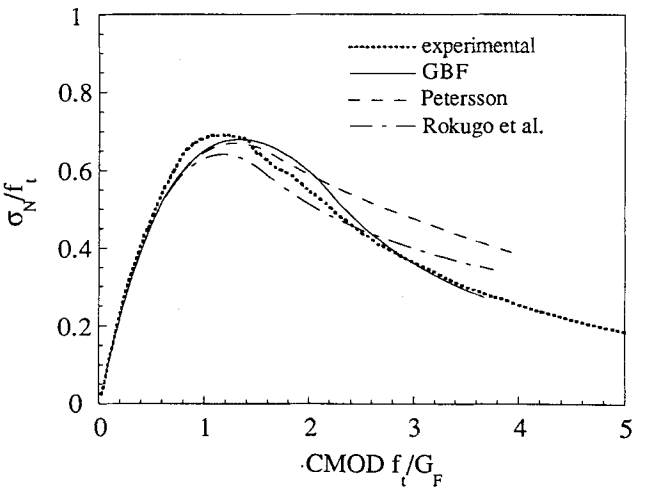

Fig. 7 Load–CMOD curves for D = 100 mm specimen.

predictions in the post-peak region were better than previous bilinear diagrams with a shorter w_c. Similar findings are quoted by Rokugo *et al.* [16] who used a bilinear diagram with a larger w_c (5 G_F/f_t) than the Petersson critical opening (w_c = 3.6 G_F/f_t).

4.2 The fitting procedure

To conclude, some remarks about the proposed procedure for obtaining the four parameters are worth consideration. The first point to discuss is the approximation of the 'true' tensile strength f_t by the cylinder splitting strength f_s. As already mentioned, the error involved in this approximation is dependent on the cylinder size and on the material fracture properties. The size dependence of the cylinder splitting strength has received renewed attention in recent years [19–21]. However, there is not yet general agreement on how to evaluate the size effect based on fracture properties. One of the reasons is that in the experimental work described by Hasegawa *et al.* [19] and Bazant *et al.* [20] the fracture properties of the concrete were not determined and therefore the results are hardly applicable to other concretes. On the other hand, Modéer [22] performed a theoretical prediction of the size effect of the cube splitting strength using the cohesive crack model but, as pointed out by Modéer himself, the results may be taken only as indicative because a number of simplifications were used in the calculations. Nevertheless, the main trend of the computation and of the experiments may coincide in showing a decreasing value of f_s with increasing size that eventually reaches a plateau. According to the theoretical model this plateau is asymptotically approached, and in the asymptotic limit $f_s = f_t$. The open problem is how fast the limiting value is approached.

A different theoretical interpretation of the size effect was given by Tang *et al.* [21] based on the two-parameter model of Jenq and Shah [23], but their computational results were obtained for particular values of the fracture parameters. Moreover, the results do not correlate directly with the tensile strength, because this is not a basic property of the two-parameter model. If the results of Modéer are taken as a reference one may expect that the splitting strength will differ by less than 15% from the true tensile strength for standard cylinders (150 mm in diameter) whenever l_{ch} is smaller than roughly 300 mm, which is the case for many concretes. This is consistent with the results presented by Mihashi [24] comparing the splitting strength with the value of f_t obtained by the indirect fitting procedure described by Wittmann *et al.* [9, 10]. Therefore, although further research on the effect of size on the splitting strength and its relationship with the true tensile strength is required, the proposed approximation may be acceptable for practical purposes, especially if one realizes that the cohesive crack model and bilinear softening are themselves approximations of the actual behaviour.

Second, to measure G_F it was necessary to refine the standard RILEM recommendation [2] by taking into account the improvements reported [4–6] where weight compensation was used. To determine the abscissa of the centroid of the area of the softening curve, careful measurements of the tail of the load–displacement curve are needed, for which purpose weight compensation is essential. Finally, to find w_1, several specimen sizes have to be tested to check that they are inside the interval where the linear approximation for the softening function suffices. This is automatically confirmed if the experimental size-effect results lie on a curve obtained by horizontally shifting the master curve in Fig. 4. In addition, it is possible to check this point by computation once the softening function is obtained. Indeed, running the calculation using a linear softening function with intercept w_1, it is enough to check that for the largest size the peak load occurs before the opening at the notch tip reaches the kink point value.

To sum up, this novel procedure allows the determination of a four-parameter bilinear softening function from tests on notched beams. These tests are easy to perform, and the proposed softening function (GBF) has proved to be a useful tool for modelling cohesive materials since not only can it reproduce peak values but also it is in good agreement with far post-peak experimental results. This is an advantage when large sizes are considered, and may be essential when pull-out of aggregates or fibres leads to very long-tailed softening diagrams.

ACKNOWLEDGEMENTS

The authors acknowledge financial support for this research from Dirección General de Investigación Científica Técnica, DGICYT, Spain, under Grant Nos. PB90-0276 and MAT90-1153-E.

APPENDIX

The explicit expressions for bilinear softening as a function of the four parameters (f_t, G_F, $\bar{w}$ and w_1) are the following:

$$\sigma = f_t\left(1 - \frac{w}{w_1}\right) \qquad \text{for } 0 \le w \le w_k$$

$$\sigma = \sigma_k\left(\frac{w - w_c}{w_k - w_c}\right) \qquad \text{for } w_k \le w \le w_c$$

$$\sigma = 0 \qquad \text{for } w \ge w_c$$

where (σ_k, w_k) are the coordinates of the kink point, given by

$$w_k = w_1 \frac{w_c - 2(G_F/f_t)}{w_c - w_1} \qquad \sigma_k = f_t \frac{2(G_F/f_t) - w_1}{w_c - w_1}$$

and w_c the critical opening, obtained from the quadratic equation

$$w_c^2 - w_c \frac{6\bar{w}(G_F/f_t) - 2w_1(G_F/f_t)}{2(G_F/f_t) - w_1} + \frac{6\bar{w}w_1(G_F/f_t) - 4w_1(G_F/f_t)^2}{2(G_F/f_t) - w_1} = 0$$

REFERENCES

1. Hillerborg, A., Modéer, M. and Petersson, P. E., 'Analysis of crack formation and crack growth in concrete by

means of fracture mechanics and finite elements', *Cem. Concr. Res.* **6** (1976) 773–782.
2. RILEM 50-FMC Recommendation, 'Determination of fracture energy of mortar and concrete by means of three-point bend test on notched beams', *Mater. Struct.* **18** (1985) 285–290.
3. Hillerborg, A., 'Results of three comparative test series for determining the fracture energy G_F of concrete', *ibid.* **18** (1985) 407–413.
4. Guinea, G. V., Planas, J. and Elices, M., 'Measurement of the fracture energy using three-point bend tests: 1. Influence of experimental procedures', *ibid.* **25** (1992) 212–218.
5. Planas, J., Elices, M. and Guinea, G. V., 'Measurement of the fracture energy using three-point bend tests: 2. Influence of bulk energy dissipation', *ibid.* **25** (1992) 305–312.
6. Elices, M., Guinea, G. V. and Planas, J., 'Measurement of the fracture energy using three-point bend tests: 3. Influence of cutting the P–δ tail', *ibid.* **25** (1992) 327–334.
7. Reinhardt, H. W., Cornelissen, H. A. W. and Hordijk, D. A., 'Tensile tests and failure analysis of concrete', *J. Struct. Engng ASCE* **112**(11) (1986) 2462–2477.
8. van Mier, J. G. M., 'Fracture of concrete under complex stress', *Heron* **31**(3) (1986) 2–90.
9. Wittmann, F. H., Rokugo, K., Bruhwiler, E., Mihashi, H. and Simoni, P., 'Fracture energy and strain softening of concrete as determined by means of compact tension specimens', *Mater. Struct.* **21** (1988) 21–32.
10. Wittmann, F. H., Roelfstra, P. E., Mihashi, H., Huang, Y. Y., Zhang, X. H. and Nomura, N., 'Influence of age of loading, water–cement ratio, and rate of loading on fracture energy of concrete', *ibid.* **20** (1987) 103–110.
11. Maturana, P., Planas, J. and Elices, M., 'Evolution of fracture behaviour of saturated concrete in the low temperature range', *Engng Fract. Mech.* **35** (1990) 827–834.
12. Dutron, P., 'Mise au point d'une composition de béton de référence pour recherches et essais en laboratoire', *Mater. Struct.* **7** (1974) 207–224.
13. Petersson, P. E., 'Crack growth and development of fracture zone in plain concrete and similar materials', Report TVBM-1006 (Division of Building Materials, Lund Institute of Technology, 1981).
14. Planas, J. and Elices, M., 'Size effect in concrete structures: Mathematical approximations and experimental validations', in 'Cracking and Damage, Strain Localization and Size Effect', edited by J. Mazars and Z. P. Bazant (Elsevier, 1988) pp. 462–476.
15. *Idem.*, 'Nonlinear fracture of cohesive materials', *Int. J. Fract.* **51** (1991) 139–157.
16. Rokugo, K., Iwasa, M., Suzuki, T. and Koyanagi, W., 'Testing methods to determine tensile strain softening curve and fracture energy of concrete', in Proceedings of International Workshop on Fracture Toughness and Fracture Energy – Test Methods for Concrete and Rock, Sendai, 1988.
17. van Mier, J. G. M., 'Scaling in tensile and compressive fracture of concrete', in 'Applications of Fracture Mechanics to Reinforced Concrete', edited by A. Carpinteri (Elsevier, 1992) pp. 95–135.
18. Liaw, B. M., Jeang, F. L., Du, J. J., Hawkins, N. M. and Kobayashi, A., 'Improved non linear model for concrete fracture', *J. Engng Mech. ASCE* **16** (1990) 429–445.
19. Hasegawa, T., Shioy, T. and Okada, T., 'Size effect on splitting tensile strength of concrete', in Proceedings of Japan Concrete Institute 7th Conference (Japan Concrete Institute, 1985), pp. 309–312.
20. Bazant, Z. P., Kazemi, M. T., Hasegawa, T. and Mazars, J., 'Size effect in Brazilian split-cylinder tests: Measurements and fracture analysis', *ACI Mater. J.* **88**(3) (1991) 325–332.
21. Tang, T., Shah, S. P., and Ouyang, C., 'Fracture mechanics and size effect of concrete in tension', *J. Struct. Engng ASCE* **118**(11) (1992) 3169–3185.
22. Modéer, M., 'A fracture mechanics approach to the failure analysis of concrete materials', Report TVBM-1001 (Division of Building Materials, Lund Institute of Technology, 1979).
23. Jenq, Y. S. and Shah, S. P., 'A two parameter fracture model for concrete', *J. Engng Mech. ASCE* **111**(10), (1985) 1227–1241.
24. Mihashi, H., 'Material structure and tension softening properties of concrete', in 'Fracture Mechanics of Concrete Structures', edited by Z. P. Bazant (Elsevier, 1992) pp. 239–250.

RESUME

Identification d'une courbe d'amollissement bilinéaire générale pour le béton

La modélisation des fissures dans le béton par des fissures cohésives s'est avérée être un procédé très utile. Une des composantes de base du modèle est la courbe d'amollissement. Il est bien connu que la forme de cette fonction a une influence déterminante sur la réponse structurelle, en particulier sur la courbe force–déplacement.

Cet article présente une nouvelle méthode d'identification des propriétés essentielles de la courbe d'amollissement à partir d'essais sur des poutres entaillées. Une courbe d'amollissement quelconque dépendant de quatre paramètres peut être envisagée; mais l'article est centré sur une relation bilinéaire à quatre degrés de liberté. On montre que quatre paramètres géométriques essentiels de la courbe peuvent être facilement estimés à partir d'essais classiques (les essais ASTM de module élastique et de traction indirecte – brésilien – et la recommandation de la RILEM pour la mesure de l'énergie de fracture par la méthode du travail de fracture).

On applique la méthode pour déterminer ces paramètres à des résultats d'essais faits au préalable par les auteurs, et on compare les résultats obtenus pour la courbe d'amollissement GBF (de l'anglais 'general bilinear fit') avec d'autres approximations bilinéaires que l'on trouve dans la littérature. La différence la plus importante est que l'identification GBF montre une extrémité beaucoup plus longue que le reste des approximations. Le résultat essentiel est que toutes les approximations donnent une bonne prédiction de la courbe force–déplacement dans la région proche du pic de charge, mais seule l'approximation bilinéaire à longue extrémité (GBF) donne aussi une excellente prédiction des régions post-pic et post-pic lointaine.